

Optical control of topological memory based on orbital magnetization

Sergey S. Pershoguba¹ and Victor M. Yakovenko²

¹*Department of Physics and Astronomy, University of New Hampshire, Durham, New Hampshire 03824, USA*

²*JQI, Department of Physics, University of Maryland, College Park, Maryland 20742, USA*

(Dated: June 1, 2021)

Motivated by twisted graphene multilayers, we study interaction of a Chern insulator with circularly polarized light. We find that the interaction energy contains an antisymmetric term that couples to the helicity of incident light, $\mathbf{h} = \text{Im}[\mathbf{E}(\omega) \times \mathbf{E}^*(\omega)]$. For a two-band Chern insulator, this term is expressed as an integral involving the Berry curvature of the system. Taking advantage of this coupling energy, we propose an experimental protocol for switching topological memory based on orbital magnetization of a Chern insulator by circularly polarized light.

Introduction. There has been much interest in heterostructures of twisted graphene multilayers [1–9]. At a small interlayer twist angle $\sim 1^\circ$, they form a periodic moiré superlattice with a large unit cell size $a \sim 10$ nm and exhibit flat electronic energy bands [1]. Therefore these systems provide a versatile and highly-tunable platform for studying electron correlations. Among many interesting phases [2–4], Chern insulators were recently identified [5–9]. They originate from spontaneous valley polarization induced by electronic correlations, resulting in orbital magnetization due to the incipient Berry curvature of graphene [10]. The orbital nature offers unique ways to control magnetization \mathbf{M} in these systems. Experiments [5–9] have demonstrated that the sign of \mathbf{M} can be switched by weak pulses of electric or magnetic fields, or electric currents, thus realizing non-volatile topological memory [8].

In this Letter, we propose to expand the toolkit for writing (and reading) of topological memory using optics. Consider circularly polarized light normally incident onto the surface of a twisted graphene Chern insulator, as shown in Fig. 1. Its helicity \mathbf{h} , parallel to the direction of light propagation, acts as an effective magnetic field. It couples to orbital magnetization \mathbf{M} of the Chern insulator, which is perpendicular to the layers. The sign of interaction energy is determined by $\mathbf{h} \cdot \mathbf{M}$, thus helicity of light makes one sign of \mathbf{M} energetically favorable, which can switch the memory.

Magnetization reversal by pulsed circularly polarized laser radiation was first demonstrated in GdFeCo magnetic films [11]. However, microscopic mechanism of this effect in spin-based magnets is subject to debate [12]. Here we focus on Chern insulators, expecting stronger electric-dipole coupling to light due to their orbital nature, in contrast to weaker magnetic-dipole interaction with spin. Our study of interaction between orbital magnetization and circularly polarized light is general and not limited to twisted graphene multilayers. We start with a symmetry analysis in the framework of the ac Stark effect, followed by a proposed experimental protocol. Then we present microscopic calculations for a two-band model and express optical response in terms of Berry curvature and Chern number. We conclude

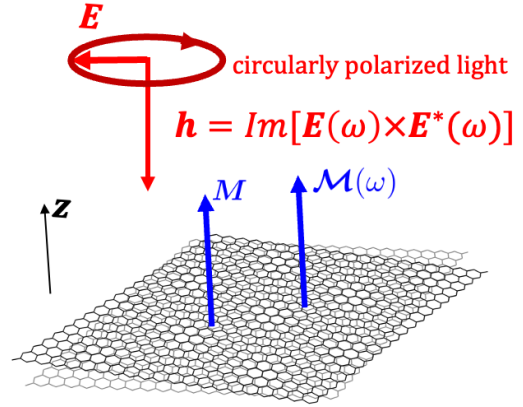


FIG. 1. Experimental setup for controlling orbital magnetization \mathbf{M} of a Chern insulator by circularly polarized light.

with applications to twisted graphene multilayers.

Phenomenological symmetry analysis. Suppose a monochromatic ac electric field $\mathbf{E}(t) = [\mathbf{E}(\omega) e^{-i\omega t} + \mathbf{E}(-\omega) e^{i\omega t}] / 2$, where $\mathbf{E}(-\omega) = \mathbf{E}^*(\omega)$, is applied to the system. The ac Stark effect [13] is the corresponding change ΔU of the energy of the system

$$\Delta U = -\frac{1}{2} E_\alpha(\omega) E_\beta(-\omega) \chi^{\alpha\beta}(\omega) \equiv U_s + U_a, \quad (1)$$

$$U_s = -\frac{1}{2} \text{Re} [E_\alpha(\omega) E_\beta^*(\omega)] \chi_s^{\alpha\beta}(\omega), \quad (2)$$

$$U_a = -\frac{i}{2} \text{Im} [E_\alpha(\omega) E_\beta^*(\omega)] \chi_a^{\alpha\beta}(\omega). \quad (3)$$

Here α and β are the Cartesian indices in three dimensions (3D). In Eqs. (2) and (3), we expanded the permittivity tensor $\chi^{\alpha\beta}$ into symmetric $\chi_s^{\alpha\beta} = (\chi^{\alpha\beta} + \chi^{\beta\alpha})/2$ and antisymmetric $\chi_a^{\alpha\beta} = (\chi^{\alpha\beta} - \chi^{\beta\alpha})/2$ parts, and introduced the corresponding contributions U_s and U_a to the energy shift. The symmetric contribution U_s represents the conventional ac Stark energy shift [13] of no interest to us. The antisymmetric contribution U_a is less common and is permitted only in the systems with broken time-reversal symmetry. The Onsager symmetry relations require that the symmetric tensor $\chi_s^{\alpha\beta}(\omega) = \chi_s^{\alpha\beta}(-\omega)$ is even, whereas the antisymmetric tensor $\chi_a^{\alpha\beta}(\omega) = -\chi_a^{\alpha\beta}(-\omega)$ is odd upon time rever-

sal. To the best of our knowledge, Pitaevskii [14] was the first to identify the antisymmetric part $\chi_a^{\alpha\beta}$ in the presence of an external magnetic field \mathbf{B} . The recently discovered orbital Chern insulators [5–9] break time-reversal symmetry spontaneously and, thus, should have a non-zero $\chi_a^{\alpha\beta}$, which is the subject of our work. It is instructive to represent the antisymmetric tensor $\chi_a^{\alpha\beta}(\omega) = i\epsilon^{\alpha\beta\gamma} \mathcal{M}_\gamma(\omega)$ via a dual vector $\mathcal{M}(\omega)$, where $\epsilon^{\alpha\beta\gamma}$ is the totally antisymmetric tensor in 3D. Then the corresponding energy contribution is

$$U_a = \frac{1}{2} \text{Im} [\mathbf{E}(\omega) \times \mathbf{E}(-\omega)] \cdot \mathcal{M}(\omega). \quad (4)$$

Since $\mathcal{M}(\omega)$ is an odd function of frequency ω , we can write it at low ω as $\mathcal{M}(\omega) \approx \omega \mathcal{M}'(0)$. Thus, in time domain for slowly changing $\mathbf{E}(t)$, Eq. (4) becomes

$$U_a = \langle \partial_t \mathbf{E}(t) \times \mathbf{E}(t) \rangle_t \cdot \mathcal{M}'(0), \quad (5)$$

where $\langle \dots \rangle_t$ denotes time averaging. Equations (4) and (5) show that the sign of the energy U_a is determined by the scalar product of the vector $\mathcal{M}(\omega)$ characterizing the system and the helicity $\mathbf{h} = \text{Im} [\mathbf{E}(\omega) \times \mathbf{E}^*(\omega)] \parallel [\partial_t \mathbf{E}(t) \times \mathbf{E}(t)]$ of circularly polarized electric field. The vector $\mathcal{M}(\omega)$ is a time-reversal-odd axial vector, so it has the same symmetry as the static magnetization \mathbf{M} of the system. Both $\mathcal{M}(\omega)$ and \mathbf{M} originate from Berry curvature (as derived later in the paper), but they are not equivalent. For two-dimensional (2D) twisted graphene multilayers, the vectors \mathbf{M} and $\mathcal{M} = \mathcal{M}\hat{\mathbf{z}}$ are parallel to z axis in Fig. 1, so Eq. (4) becomes $U_a = \mathcal{M}(\omega) \text{Im} [\mathbf{E}(\omega) \times \mathbf{E}^*(\omega)]_z / 2$. Below we present an experimental protocol for optical control of the sign of orbital magnetization that does not involve a quantitative estimate of $\mathcal{M}(\omega)$.

Experimental protocol. The Chern insulator state develops as the second-order phase transition at $T_c = 7.5$ K [8], where the system spontaneously breaks time-reversal symmetry. Either \mathcal{M} or \mathbf{M} or the Hall resistance R_{xy} can be taken as the order parameter, having positive or negative sign. The experimentally measured sign of R_{xy} can represent topological memory.

We propose to irradiate the system by circularly polarized light, which is likely to produce heating and raise the sample temperature T above T_c . So, we suggest to take advantage of this parasitic heating and use laser power to control T following the protocol sketched in Fig. 2. The three panels show laser power, the sample temperature T , and the Hall resistance R_{xy} versus time t of the experiment.

At $t = 0$, we start at a high laser power, so that $T > T_c$ and $R_{xy} = 0$. Then we gradually decrease laser power, which lowers T until it reaches T_c at $t = t_1$, when the sample undergoes transition into the Chern insulator phase. The presence of circularly polarized light breaks symmetry between the two, otherwise equienergetic, states of the system characterized by opposite

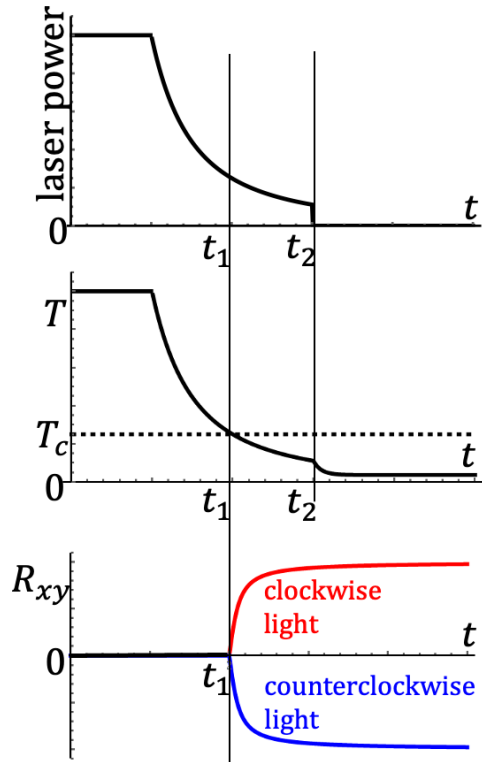


FIG. 2. Experimental protocol, showing laser power, sample temperature T , and Hall resistance R_{xy} versus time t . Decreasing laser power lowers T and drives the sample through transition at T_c . The sign of resultant Hall resistance R_{xy} is determined by helicity of circularly polarized light.

signs of R_{xy} . The system chooses the state of lower energy U_a , as determined by helicity of incident light in Eq. (4), which is manifested in the sign of measured R_{xy} . Since the Landau energy at the second-order phase transition is quadratic in \mathcal{M} , whereas U_a is linear in \mathcal{M} , even a weak electric field \mathbf{E} in Eq. (4) is sufficient to control symmetry breaking. Once T decreases well below T_c , laser power can be turned off at $t = t_2$, but the sign of R_{xy} stays the same.

Effectively, the circularly polarized light acts as a “training field” that forces the system to choose a particular sign during symmetry breaking. It is similar to a small training magnetic field applied to control the sign of spontaneously developing polar Kerr effect at the superconducting transition in Sr_2RuO_4 , which breaks time-reversal symmetry [15]. The read-out of the sign of R_{xy} in Chern insulators can also be carried out optically by measuring the polar Kerr effect.

Microscopic derivation. Here we present a microscopic derivation of the magnetic vector $\mathcal{M}(\omega)$ appearing in Eq. (4). We start with a generic Hamiltonian $H = H_0 + V(t)$, consisting of the bare term H_0 and the time-dependent term $V(t) = e\mathbf{r} \cdot \mathbf{E}(t)$, which represents dipolar coupling to an oscillating electric field

$E(t)$. Then we evaluate the ac Stark energy shift to the second order in the electric field. We use the conventional time-dependent perturbation theory [16] and evaluate both the symmetric and antisymmetric parts of the permittivity tensor (see details in Sec. I of Supplemental Material [17])

$$\begin{aligned}\chi_s^{\alpha\beta}(\omega) &= \sum_{\substack{m \in \{\text{emp}\} \\ n \in \{\text{occ}\}}} \frac{(\varepsilon_n - \varepsilon_m) \text{Re}(r_{nm}^\alpha r_{mn}^\beta) e^2}{(\varepsilon_n - \varepsilon_m + i\delta)^2 - (\hbar\omega)^2}, \\ \chi_a^{\alpha\beta}(\omega) &= \sum_{\substack{m \in \{\text{emp}\} \\ n \in \{\text{occ}\}}} \frac{i \hbar\omega \text{Im}(r_{nm}^\alpha r_{mn}^\beta) e^2}{(\varepsilon_n - \varepsilon_m + i\delta)^2 - (\hbar\omega)^2}.\end{aligned}\quad (6)$$

Here the double summation runs over the occupied and empty electronic states of the energies ε_n and ε_m labeled by the indices n and m , respectively. The matrix elements of the coordinate r_{mn}^α are evaluated with respect to these states. The small parameter $\delta > 0$ simulates adiabatic onset of $V(t)$. The symmetric tensor $\chi_s^{\alpha\beta}(\omega)$ reproduces the conventional ac Stark energy shift [13], whereas we focus on the antisymmetric tensor $\chi_a^{\alpha\beta}(\omega)$. Equations (6) are written for $T = 0$, but can be easily generalized to non-zero temperature by introducing the Fermi occupation functions.

Now let us simplify $\chi_a^{\alpha\beta}(\omega)$ in Eq. (6) for a two-band Chern insulator (details are given in Sec. II of Supplemental Material [17]). In this case, the single-particle states are indexed by the continuous quasimomentum \mathbf{k} , as well as the indices o and e for the occupied and empty bands. The corresponding eigenenergies and Bloch wavefunctions are $\varepsilon_{o(e)}(\mathbf{k})$ and $\psi_{o(e),\mathbf{k}}(\mathbf{r}) = e^{i\mathbf{k}\mathbf{r}} u_{o(e),\mathbf{k}}(\mathbf{r})$. For a spatially uniform electric field $\mathbf{E}(t)$, the perturbation $V(t)$ has only “vertical” interband matrix elements between the states ψ_{o,\mathbf{k}_1} and ψ_{e,\mathbf{k}_2} with $\mathbf{k}_1 = \mathbf{k}_2$. It is well known [18, 19] that these matrix elements represent the interband Berry connections, i.e., $r_{oe}^\alpha(\mathbf{k}) = i \langle u_{o,\mathbf{k}} | \partial^\alpha u_{e,\mathbf{k}} \rangle$, where $\partial^\alpha = \partial / \partial k_\alpha$ denotes the momentum derivative. Furthermore, the product of the two matrix elements $\text{Im}[r_{oe}^\alpha r_{eo}^\beta] = -\epsilon^{\alpha\beta\gamma} \Omega_{o,\gamma}(\mathbf{k})/2$ is expressed via the Berry curvature of the occupied band $\Omega_{o,\gamma}(\mathbf{k}) = i \epsilon_{\alpha\beta\gamma} \langle \partial^\alpha u_{o,\mathbf{k}} | \partial^\beta u_{o,\mathbf{k}} \rangle$. In the case of a planar 2D system, e.g., twisted graphene, the Berry vector $\boldsymbol{\Omega}_o = \Omega_o \hat{z}$ is parallel to z axis. Then, recalling the representation $\chi_a^{\alpha\beta}(\omega) = i \epsilon^{\alpha\beta z} \mathcal{M}(\omega)$, we obtain from Eq. (6)

$$\frac{\mathcal{M}(\omega)}{\mathcal{A}} = \frac{e^2}{2} \int \frac{d^2k}{(2\pi)^2} \frac{\hbar\omega \Omega_o(\mathbf{k})}{[\varepsilon_o(\mathbf{k}) - \varepsilon_e(\mathbf{k}) + i\delta]^2 - (\hbar\omega)^2}, \quad (7)$$

where \mathcal{A} is the area of the system.

Let us examine the asymptotic behavior of Eq. (7) at low and high frequencies. At low subgap frequencies $\hbar\omega \ll |\varepsilon_e(\mathbf{k}) - \varepsilon_o(\mathbf{k})|$, we can drop ω in the denominator

$$\frac{\mathcal{M}(\omega)}{\mathcal{A}} \approx \frac{e^2 \hbar\omega}{2} \int \frac{d^2k}{(2\pi)^2} \frac{\Omega_o(\mathbf{k})}{[\varepsilon_e(\mathbf{k}) - \varepsilon_o(\mathbf{k})]^2}. \quad (8)$$

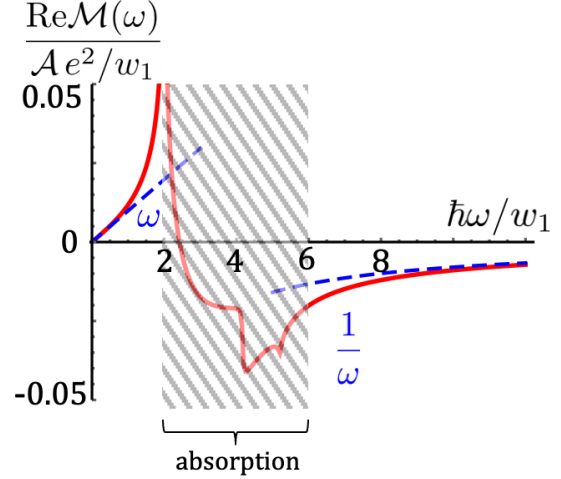


FIG. 3. Frequency dependence of $\text{Re}\mathcal{M}(\omega)$ in Eq. (4) for the antisymmetric ac Stark effect, calculated from Eq. (7) for the topological Haldane model. The low and high frequency asymptotes from Eqs. (8) and (9) are shown by dashed lines.

The integral in Eq. (8) determines the coefficient $\mathcal{M}'(0)$, in Eq. (5). At high frequencies $\hbar\omega \gg |\varepsilon_e(\mathbf{k}) - \varepsilon_o(\mathbf{k})|$, we obtain

$$\frac{\mathcal{M}(\omega)}{\mathcal{A}} \approx -\frac{e^2}{4\pi} \left(\frac{C}{\hbar\omega} + \frac{D}{(\hbar\omega)^3} \right), \quad (9)$$

$$C = \int \frac{d^2k}{2\pi} \Omega_o(\mathbf{k}), \quad D = \int \frac{d^2k}{2\pi} \Omega_o(\mathbf{k}) [\varepsilon_e(\mathbf{k}) - \varepsilon_o(\mathbf{k})]^2.$$

Comparing Eqs. (8) and (9), we observe that $\mathcal{M}(\omega)$ has opposite signs in the low and high frequency limits. Interestingly, the leading term C/ω in Eq. (9) depends only on the integer topological Chern number C , which determines the quantized Hall conductance $R_{xy}^{-1} = Ce^2/h$ of the edge states. If the Chern number vanishes, $C = 0$, then the leading term is D/ω^3 , consistent with an earlier calculation [20] of the bulk ac Hall conductivity $\sigma_{xy}(\omega)$ for a two-band model. Interplay between edge and bulk contributions is discussed in more detail in Sec. III of Supplemental Material [17].

At intermediate frequencies, the energy denominator in Eq. (7) may vanish at $\hbar\omega = |\varepsilon_2(\mathbf{k}) - \varepsilon_1(\mathbf{k})|$. It produces an imaginary part of $\mathcal{M}(\omega)$, which physically represents resonant interband absorption. Although it is not the main focus of our work, we note that this absorption is also dependent on the magnetic state of the system via the Berry curvature. The real and imaginary parts of $\mathcal{M}(\omega)$ are related by the appropriate Kramers-Kronig relation.

As an illustration, frequency dependence of the real part of $\mathcal{M}(\omega)$, calculated from Eq. (7) for the well-known Haldane model [21], is shown in Fig. 3 (details are given in Sec. IV of Supplemental Material [17]). The nearest-neighbor and next-nearest-neighbor tunnelling amplitudes w_1 and iw_2 on the honeycomb lattice are selected to be real and imaginary with the magnitudes

$w_2 = w_1/2$, so that the Chern number is $C = 1$. At low and high frequencies, Fig. 3 illustrates the ω and $1/\omega$ asymptotic behavior from Eqs. (8) and (9). At the intermediate frequencies $2w_1 < \hbar\omega < 6w_1$, where resonant absorption is possible, $\text{Re}\mathcal{M}(\omega)$ exhibits a series of kinks and dips associated with band edges and van Hove singularities in the density of states.

The static ($\omega = 0$) orbital magnetization M of a Chern insulator can also be expressed as an integral involving Berry curvature [22, 23]. However, the integrals for M and for $\mathcal{M}(\omega)$ in Eq. (7) are different. Thus, M and $\mathcal{M}(\omega)$ are not equivalent, but their signs are both determined by the sign of the Berry curvature $\Omega_o(\mathbf{k})$.

Application to twisted graphene multilayers. We follow theoretical models [10, 24, 25] of a twisted graphene bilayer on the boron nitride (BN) substrate. The low-energy model [10] consists of two bands per valley (K or K') of graphene, separated by the energy gap Δ induced by the BN substrate and carrying Chern numbers $C = \pm 1$ of opposite signs. At the filling factor $\nu = 4$ per moiré unit cell, four bands above the gap are fully occupied (for valleys K and K' , and spins up and down), so the system is a trivial band insulator. In contrast, at $\nu = 3$, Coulomb interaction between electrons induces spontaneous valley polarization. In that state, the two bands of, e.g., K' valley are fully occupied, whereas one band of K valley (with a given spin orientation) rises above the Fermi level and becomes empty (see Fig. 1(c) in Ref. [7]). This empty band and the corresponding filled band of the same spin orientation below the gap Δ map onto the Haldane model [24]. Therefore, our Eqs. (7)–(9) for a two-band model are qualitatively applicable to the twisted graphene bilayer on BN.

Let us crudely estimate the magnitude of the proposed effect. Given that $\mathcal{M}(\omega)$ decreases both at low and high frequencies in Eqs. (8) and (9), the maximal $\mathcal{M}(\omega)$ is achieved at the optimal frequency of the order of bandgap, i.e., at $\hbar\omega \sim \Delta$. Then the antisymmetric ac Stark energy shift per unit cell \tilde{U}_a can be estimated as $\tilde{U}_a \sim (eEa)^2 C / 4\pi\Delta$ at the optimal frequency, where a is the unit cell size. Taking the characteristic values $\Delta \sim 1$ meV, $a \sim 10$ nm, $C = 1$, and $E = 3 \times 10^4$ V/m (for a 0.01 W laser with the spot size $d = 0.1$ mm), we find the Stark energy $\tilde{U}_a^{(1)} \sim 8 \times 10^{-6}$ eV. For a laser of visible light $\hbar\omega \sim 2$ eV, that estimate is reduced by a factor of $\Delta/\hbar\omega \sim 5 \times 10^{-4}$ from Eq. (9), thus producing $\tilde{U}_a^{(2)} \sim 4 \times 10^{-9}$ eV. It is instructive to compare these estimates with a typical energy shift induced by the magnetic field $\mu_B B \sim 5.8 \times 10^{-5}$ eV $\times B[\text{T}]$ per unit cell carrying a magnetic moment of the order of Bohr magneton [8]. The two estimates $\tilde{U}_a^{(1)}$ and $\tilde{U}_a^{(2)}$ correspond to the effective magnetic fields $B^{(1)} \sim 0.1$ T and $B^{(2)} \sim 0.6$ G, respectively. In experiment [8], magnetization was switched by a magnetic field as low as $B = 0.08$ T. These estimates show that the effect of circularly polarized light is comparable to the mag-

netic fields used in experiments [7, 8] to control magnetization. The estimates can be greatly enhanced by increasing pulsed laser power [11]. If heating becomes a problem, the experimental protocol described earlier can be employed.

Conclusions. For the systems that break time-reversal symmetry, the energy of interaction with an external ac electric field $\mathbf{E}(\omega)$ contains an antisymmetric term (4) that couples to the helicity of circularly polarized light $\mathbf{h} = \text{Im}[\mathbf{E}(\omega) \times \mathbf{E}^*(\omega)]$. This term is distinct from the usual symmetric ac Stark energy shift present in any system. For a two-band Chern insulator, the coefficient $\mathcal{M}(\omega)$ in the antisymmetric term (4) is expressed as an integral over the Brillouin zone (7) involving the Berry curvature $\Omega_o(\mathbf{k})$ of the lower, occupied band. Taking advantage of this interaction energy, we propose an experimental protocol for switching orbital magnetization of a Chern insulator using circularly polarized light as shown in Fig. 2. Gradual decrease of laser power lowers the sample temperature from $T > T_c$ to $T < T_c$ and drives the system through the time-reversal breaking transition at T_c . The helicity of circularly polarized light forces the system to select a particular sign of the orbital magnetization and the spontaneous Hall resistance R_{xy} at the transition, thus realizing optical control of topological memory.

We would like to thank G. Polshyn for stimulating discussions that motivated this work. SP was supported by the U.S. Department of Energy (DOE), Office of Science, Basic Energy Sciences (BES) under Award No. DE-SC0020221.

-
- [1] R. Bistritzer and A. H. MacDonald, “Moiré bands in twisted double-layer graphene,” *PNAS* **108**, 12233 (2011).
 - [2] Y. Cao, V. Fatemi, S. Fang, K. Watanabe, T. Taniguchi, E. Kaxiras, and P. Jarillo-Herrero, “Unconventional superconductivity in magic-angle graphene superlattices,” *Nature* **556**, 43 (2018).
 - [3] Y. Cao, V. Fatemi, A. Demir, S. Fang, S. L. Tomarken, J. Y. Luo, J. D. Sanchez-Yamagishi, K. Watanabe, T. Taniguchi, E. Kaxiras, R. C. Ashoori, and Jarillo-Herrero. P., “Correlated insulator behaviour at half-filling in magic-angle graphene superlattices,” *Nature* **556**, 80 (2018).
 - [4] M. Yankowitz, S. Chen, H. Polshyn, Y. Zhang, K. Watanabe, T. Taniguchi, D. Graf, A. F. Young, and C. R. Dean, “Tuning superconductivity in twisted bilayer graphene,” *Science* **363**, 1059 (2019).
 - [5] A. L. Sharpe, E. J. Fox, A. W. Barnard, J. Finney, K. Watanabe, T. Taniguchi, M. A. Kastner, and D. Goldhaber-Gordon, “Emergent ferromagnetism near three-quarters filling in twisted bilayer graphene,” *Science* **365**, 605 (2019).
 - [6] X. Lu, P. Stepanov, W. Yang, M. Xie, A. M. Ali, I. Das, C. Urgell, C. Watanabe, T. Taniguchi, G. Zhang, A. Bachtold, A. MacDonald, and D. K. Efetov, “Su-

- perconductors, orbital magnets and correlated states in magic-angle bilayer graphene,” *Nature* **574**, 653 (2019).
- [7] M. Serlin, C. L. Tschirhart, H. Polshyn, Y. Zhang, J. Zhu, K. Watanabe, T. Taniguchi, L. Balents, and A. F. Young, “Intrinsic quantized anomalous Hall effect in a moiré heterostructure,” *Science* **367**, 900 (2020).
 - [8] H. Polshyn, J. Zhu, M. A. Kumar, Y. Zhang, F. Yang, C. L. Tschirhart, M. Serlin, K. Watanabe, T. Taniguchi, A. H. MacDonald, and A. F. Young, “Electrical switching of magnetic order in an orbital Chern insulator,” *Nature* **588**, 66 (2020).
 - [9] G. Chen, A. L. Sharpe, E. J. Fox, Y.-H. Zhang, S. Wang, L. Jiang, B. Lyu, H. Li, K. Watanabe, T. Taniguchi, Z. Shi, T. Senthil, D. Goldhaber-Gordon, Y. Zhang, and F. Wang, “Tunable correlated Chern insulator and ferromagnetism in a moiré superlattice,” *Nature* **579**, 56 (2020).
 - [10] J. C. W. Song, P. Samutpraphoot, and L. S. Levitov, “Topological Bloch bands in graphene superlattices,” *PNAS* **112**, 10879 (2015).
 - [11] C. D. Stanciu, F. Hansteen, A. V. Kimel, A. Kirilyuk, A. Tsukamoto, A. Itoh, and Th. Rasing, “All-Optical Magnetic Recording with Circularly Polarized Light,” *Phys. Rev. Lett.* **99**, 047601 (2007).
 - [12] E. Y. Vedmedenko, R. K. Kawakami, D. D. Sheka, P. Gambardella, A. Kirilyuk, A. Hirohata, C. Binek, O. Chubykalo-Fesenko, S. Sanvito, B. J. Kirby, J. Grollier, K. Everschor-Sitte, T. Kampfrath, C.-Y. You, and A. Berger, “The 2020 magnetism roadmap,” *J. Phys. D: Appl. Phys* **53**, 453001 (2020).
 - [13] D. H. Kobe, “Gauge invariant derivation of the AC Stark shift,” *J. Phys. B: Atom. Mol. Phys.* **16**, 1159 (1983).
 - [14] L. P. Pitaevskii, “Electric forces in a transparent dispersive medium,” *Sov. Phys. JETP* **12**, 1008 (1961).
 - [15] J. Xia, Y. Maeno, P. T. Beyersdorf, M. M. Fejer, and A. Kapitulnik, “High Resolution Polar Kerr Effect Measurements of Sr_2RuO_4 : Evidence for Broken Time-Reversal Symmetry in the Superconducting State,” *Phys. Rev. Lett.* **97**, 167002 (2006).
 - [16] J. J. Sakurai and J. J. Napolitano, *Modern Quantum Mechanics* (Pearson, 2010).
 - [17] Supplemental materials are available at “hyperlink generated by APS”.
 - [18] E. I. Blount, *Formalisms of Band Theory* in *Solid State Physics*, edited by F. Seitz and D. Turnbull, Vol. 13 (Academic Press, New York and London, 1962).
 - [19] E. M. Lifshitz and L. P. Pitaevskii, *Statistical Physics Part 2. Theory of the Condensed State. Landau and Lifshitz Course of Theoretical Physics*, Vol. 9 (Pergamon Press, 1980).
 - [20] S. Tewari, C. Zhang, V. M. Yakovenko, and S. Das Sarma, “Time-Reversal Symmetry Breaking by a $(d + id)$ Density-Wave State in Underdoped Cuprate Superconductors,” *Phys. Rev. Lett.* **100**, 217004 (2008).
 - [21] F. D. M. Haldane, “Model for a Quantum Hall Effect without Landau Levels: Condensed-Matter Realization of the “Parity Anomaly,”” *Phys. Rev. Lett.* **61**, 2015 (1988).
 - [22] D. Xiao, J. Shi, and Q. Niu, “Berry Phase Correction to Electron Density of States in Solids,” *Phys. Rev. Lett.* **95**, 137204 (2005).
 - [23] T. Thonhauser, D. Ceresoli, D. Vanderbilt, and R. Resta, “Orbital Magnetization in Periodic Insulators,” *Phys. Rev. Lett.* **95**, 137205 (2005).
 - [24] Y.-H. Zhang, D. Mao, and T. Senthil, “Twisted bilayer graphene aligned with hexagonal boron nitride: Anomalous Hall effect and a lattice model,” *Phys. Rev. Research* **1**, 033126 (2019).
 - [25] N. Bultinck, S. Chatterjee, and M. P. Zaletel, “Mechanism for Anomalous Hall Ferromagnetism in Twisted Bilayer Graphene,” *Phys. Rev. Lett.* **124**, 166601 (2020).